Anion Exchange Membranes: The Effect of Reinforcement in Water and Electrolyte

Xiaoyan Luo,[1,†,$] Douglas Kushner,[1,$] and Ahmet Kusoglu[1,*]

[1] Energy Conversion Group, Lawrence Berkeley National Laboratory (LBNL), Berkeley, CA, 94720 (USA)

† Present Address: Energy Materials Department, Suzhou Laboratory, Suzhou, Jiansu, 215123 (China)

[$] Contributed equally

*E-mail: akusoglu@lbl.gov

Abstract

Alkaline anion-conducting polymer-based CO_2 electrolysis and water electrolysis are among two emerging renewable energy conversion technologies. Their system design and integration offer promise of lower capital cost due to utilization of non-noble catalysts, in contrast to platinum group metal catalysts required for cation-conducting polymer-based devices. However, a critical component, the polymer electrolyte membrane, remains an obstacle hampering system performance and durability. In this study, commercially-available Sustainion® membranes with and without PTFE-reinforcement were investigated to understand previously unreported origins of improved device performance when compared to alternative membrane chemistries. We report critical membrane properties, such as morphology, thermal stability, as well as temperature-, hydration-, and counter-ion dependent ion conductivity. Moveover, the changes in uptake and conductivity of membranes in supporting electrolytes of K_2CO_3 and KOH investigated as a function of their concentration. Presence of reinforcement and supporting electrolyte type alter the membrane's transport functionality, which could help guide device design for improved performance. The obtained results not only show how Sustainion® properties change with operating environment for CO_2 and water electrolysis applications, but also provide understanding for internal and external factors controlling anion-exhcnage membrane functionality in electrochemical devices.

Keywords: Anion-Exchange Membrane, Reinforcement, Electrolytes, Structure-Property, Conductivity

Introduction

With increasing need and urgency to decarbonize key sectors, it is imperative to reduce and even reverse the carbon emissions using energy conversion and carbon-capture technologies.[1]ref Electrochemical water splitting and CO_2 reduction are two technologies leading the green revolution for production of fuels and value-added chemicals, capable of reducing or even capturing CO_2 emissions using renewable energy.[2-6]

Alkaline water electrolyzers (AWE) based on liquid-electrolytes have been commercially available for several decades, high internal transport resistance limits their use and potential for efficient energy conversion and storage technologies. Polymer-electrolyte membrane water electrolyzers (PEMWE) utilizing zero-gap configurations can operate at high current densities without compromising energy efficiency. PEMWE devices benefit from lower overpotential, electrolyte management, and gas purity, leading to smaller and simpler systems that promote use of small-scale hydrogen production plants.[7-10] Proton-exchange membranes (PEM) and anion-exchange membranes (AEM) are two typical classes of solid-electrolyte membranes. In PEM systems, the acidic environment makes replacing the noble expensive catalyst extremely challenging. In contrast, AEM-based water electrolysis in an alkaline environment can utilize non-precious metal catalysts (e.g. Fe, Ni or Co-based) and less expensive steel hardware (as opposed to Ti), which drives down the system cost and provides advantages over PEM-based cells.[10-12] In addition, the alkaline enviroment also favors the oxygen evolution reaction kinetics compared to the acid environment in PEM system. Moreover, AEM systems can be adapted for CO_2 electrolysis (electrochemical CO_2 reduction), mitigating problems with low solubility of CO_2 in aqueous-fed systems that limit CO_2 conversion, but also the catholyte with an anion-conducting membrane to enable higher current densities.[5, 6, 13, 14]

One of the greatest research challenges for AEMs is the polymer stability under an alkaline environment.[5, 10, 11, 15] A recently developed imidazole-functionalized AEM, Sustainion® (Figure 1), exhibits stability in strong alkaline solutions, as well as maintains lower cost due to an inexpensive polystyrene-based backbone.[6, 8, 16] In addition, Sustainion® has been used in various energy applications, including the electrochemical conversion of CO_2 to formic acid (HCOOH), CO_2 to carbon monoxide (CO), and alkaline water electrolysis.[5, 14, 17, 18] Recently, promising results were reported in CO_2 reduction utilizing Sustainion ionomers to create a bilayer to tune the catalyst micro-enviroment.[14] In addition, hydrogen generation using Sustainion® can operate at high

current densities and low voltages without using precious metal electrocatalysts.[19, 20] Therefore, Sustainion® can serve as a suitable model system for fundamental and systematic investigation of AEMs and is baselined against FAA-3 from Fumatech. The structure for FAA-3 is omitted due to lack of public disclosure but it is known to have a poly(phenylene oxide) backbone with a quaternary ammonium group attached.

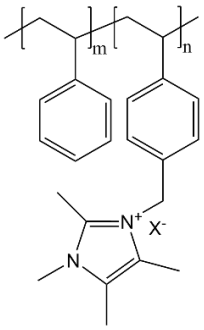

Figure 1 Chemical structure of Sustainion® with the 1,2,4,5-tetramethyl imidazole functional group where m and n are 6 and 1, respectively, and X^- is an anion such as OH^-, Cl^-, Br^-, CO_3^{-2}, HCO_3^-.

Thus far, only a few studies used Sustainion® membrane yet their focus has been on the electrochemical cell performance.[6, 19-21] Recently, water transport through Sustainion®-based CO_2 electrolyzer was quantified using an *in-situ* sensor on the cathode chamber.[22] The reports on membrane properties and their understanding; however, is far from adequate. Typical properties of Sustainion® membrane, such as ion exchange capacity (IEC), OH^- ion conductivity in liquid water, and water content have been reported.[23] However, membrane morphology, thermal-mechanical properties, as well as their correlations to conductivity properties, particularly under vapor phase for liquid-free systems, and in supporting electrolytes, are missing, despite the key role of these in cell performance. Of particular importance is the understanding of how these inter-correlations change in a membrane with reinforcement layer, which has been widely adopted in engineering applications.

The mechanical stability of an AEM is important for the durability of electrolyzers. Cross-linking and impregnating porous PTFE are the two common methods to control the membrane swelling and to enhance the membrane durability.[24] However, issues related to controlling and reducing brittleness when drying out during cross-linking makes the reinforcement strategy more

promising. Reinforcement strategies in fuel-cell PEMs, such as the commercially available Gore-Select membranes incorporating an expanded PTFE mesh into PFSA membranes, have been proven to be an effective way for the development of robust and thin membranes, (5 to 20 μm), while reducing transport resistance and cost.[25]

Numerical studies and experimental investigations found that higher temperature operation could improve cell performance by enabling lower electrolysis voltage and higher current density operation.[3, 26, 27] For water electrolyzers, operating Nafion®-based system at 80-130 °C with controlled system pressure can reduce the overpotential, albeit at the expense of membrane dehydration problems. From simulation results, AEM-based CO_2 electrolysis cell operating at a higher temperature (e.g., 80 °C) exhibits improved charge transfer kinetics, enhanced CO_2 utilization as well as reduced water transport limitations that are usually observed at room temperature.[26] Therefore, understanding membrane behavior at high temperatures is beneficial for improving the performance of these cells, particularly gas-polymer electrolyte (liquid-free type) cells, where the cathode is fed with CO_2 gas.[28] For this reason, this study examines AEM properties in water vapor conditions at higher temperatures.

In addition, supporting electrolytes (SE) were found to play a critical role in electrochemical systems, such as alkaline electrolysis or redox flow battery systems where SE combined with other cheap separators as an effective capital cost reduction option.[29] An aqueous supporting electrolyte (SE), such as KOH, is commonly used in other electrochemical cells to improve the cell performance and to eliminate the need for incorporating an ionomer binder in the catalyst layer.[30, 31] For example, 24 wt% KOH as the supporting electrolyte in alkaline water electrolyze was found to have polarization behavior comparable to PEM electrolyzer without PGM catalysts.[30] However, the impact of supporting electrolyte on transport properties and nanomorphology of Sustainion® membranes has yet to be investigated. In the study, we carry out a systematic investigation on Sustainion® membranes to study the impact of supporting electrolyte on ion transport properties and nanomorphology, examine the role of reinforcement, and provide a property data set that could help understanding of their structure-hydration-transport correlations.

2. Experimental

2.1 Materials

Sustainion® 37-50 and Sustainion® PTFE reinforced X37-50 membranes were purchased from Dioxide Materials. Fumasep FAA-3 was purchased from Fuel Cell Store. Expanded PTFE (ePTFE) was produced by 3M. As-received Sustainion® 37-50 membranes were soaked in 1 M KOH solution overnight to remove the supporting liner before the further anion-exchange process. OH^-, CO_3^{2-} and Br^- form membranes were obtained after treating membranes twice with fresh 1 M KOH, K_2CO_3, and KBr solution, respectively, and then soaked in Millipore-grade water (>18.0 MΩ-cm) to remove excess salt. IEC values for each membrane and ion form are tabulated in Table 1. All membranes were stored in an air tight container with Millipore-grade water that has been purged with CO2-free nitrogen for 5 min prior to sealing the container and purged again after each time the container was opened.

Table 1 List of membranes used in this study. The values represent the effective IEC for reinforced membrane which are calculated by accounting for the reinforcement.

Membrane	Effective IEC (mmol/g)		
	OH^-	CO_3^{2-}	Br^-
Sustainion®	1.12	1.07	1.05
Reinforced Sustainion®	1.02	0.98	0.96
Fumasep® FAA3	1.92	1.81	1.71

2.2 Dynamic Mechanical Analysis (DMA)

Membrane thermal property was studied in tension mode using a dynamic mechanical analyzer (DMA) by TA Instruments Discovery DMA 850. 8 mm wide sample was placed at the tension clamp at the lock position. Dried house N_2 gas was fed through the DMA chamber overnight to remove all the ambient water and ensure a dry state for the polymer prior to the testing. The house N_2 gas was turned off before the experiment. The sample was strained between a fixed and a moving clamp in a static oscillation load. The sample was then tested at the frequency of 1.0 Hz with a temperature sweep from room temperature to sample failure at a ramping rate of 5 °C/min. From the collected stress-temperature data, storage modulus (E), loss modulus, and their ratio or tan(δ) were determined.

142

143 **2.3 Thermogravimetric Analysis**

144 The thermogravimetric analysis (TGA) was carried out using a Perkin Elmer TGA 4000 instrument.
145 An analytical balance and a controlled-atmosphere oven were coupled to measure a sample's mass
146 loss as a function of temperature (from ambient ca. 25 °C to 700 °C) at a constant heating rate of
147 10 °C/min in dry nitrogen purge gas. The instrument had a sample temperature precision of ±
148 0.4 °C and a balance accuracy of ± 0.02%. Two type of experiments were carried out using the
149 TGA. First, a hydrated sample with mass of ~8-20 mg was tested after blotted the surface water
150 with Kimwipe. Between each test, careful cleaning was performed by holding the temperature at
151 900 °C for 10 minutes under the air atmosphere to oxidize all residue.

152 Then, another test was performed to determine the PTFE mass loading in reinforced membranes
153 by comparing the mass loss curves of membranes in CO_3^{2-} form using the following procedure.
154 First, the samples were heated to 120 °C at 5 °C/min followed by an isothermal hold for 30 min to
155 remove water from each sample. The samples were then cooled to 30 °C at 50 °C/min followed
156 by another isothermal hold for 15 min. The final step consisted heating the samples to 750 °C at a
157 rate of 5 °C/min. The mass fraction of the PTFE reinforcement, f_r, was determined from the
158 difference in the mass loss at 500 °C. From the calculated mass of the reinforcement layer, an
159 effective EW is determined for the reinforced membrane using the expression: $EW' = EW *$
160 $(1 - f_r)$.

161 **2.4 Membrane Density**

162 The dry membrane density (ρ_{dry}) was used to calculate the membrane volume fraction, which is
163 determined using an Ohaus density determination kit at room temperature. All the membranes
164 were dried in a vacuum oven overnight at 70 °C and then cooled to room temperature prior to
165 measurement. An Ohaus Adventurer® balance was used to obtain the sample mass in air and in the
166 auxiliary liquid (i.e., decane). The dry sample density was calculated according to:[32]

167 $$\rho_{dry} = \frac{W_A}{W_A - W_B}(\rho_0 - \rho_L) + \rho_L \quad (1)$$

168

169 where W_A and W_B are the sample weight in air and in the auxiliary liquid. ρ_0 and ρ_L are the density
170 of the auxiliary liquid and air, respectively.

2.5 Water-sorption Behavior

Isothermal water vapor sorption of the membrane was measured using a dynamic vapor sorption analyzer (DVS Surface Measurement Systems, UK) with temperature and humidity control. The samples were humidified from 0 to 98% RH, and then dehumidified from 98% to 0% with increments of 10% RH at 25 °C. The humidified membrane weight (W_{RH}) was determined at each RH step after the mass gain reached a steady-state (dm/dt < 0.005 %/min.). The dry weight (W_{dry}) of the humidified membrane was obtained after drying the anion-exchange membrane at 0% RH at 25 °C in the DVS. The details of the experimental procedure can be found in a previous study.[32] The percent water uptake (WU) by weight was calculated from the measured weight:

$$WU = \frac{W_{RH} - W_{\mathrm{dry}}}{W_{\mathrm{dry}}} \times 100 \quad (2)$$

From the water uptake measured during sorption, WU_{sorption}, and desorption, $WU_{\mathrm{desorption}}$, sorption hysteresis in the vapor phase (Δ_{WU}) was calculated as follows:

$$\Delta_{WU} = WU_{\mathrm{desorption}} - WU_{\mathrm{sorption}} \quad (3)$$

In addition, liquid water sorption measurement was carried out by soaking the membrane in liquid water for at least three days and then measuring its wet weight (W_{wet}), after blot dried the surface water. Dry weight (W_{dry}) of the wet membrane was determined after vacuum drying the samples at 110 °C overnight and cooling in a desiccator, and water uptake in liquid water is calculated using Equation 3. To characterize hydration, water content, λ, is calculated from the average of water uptake during sorption and desorption:

$$\lambda = \frac{\mathrm{mol\ H_2O}}{\mathrm{mol\ Ion}} = \frac{(W_{RH} - W_{\mathrm{dry}})}{W_{\mathrm{dry}} * M_{H_2O}} \frac{EW'}{M_{H_2O}} \quad (4)$$

where EW', is determined from the IEC (mmol/g) values reported in Table 1 and discussed in the previous section on TGA, and M_{H_2O} is the molar mass of water (18 g/cm^3).

2.6 Membrane Conductivity

A sample with a dimension of 10 mm × 35 mm was loaded to a four-probe in-plane conductivity cell to measure conductivity. For conductivity in water vapor, a membrane testing system (MTS 740, Scribner Associates Inc.) equipped with a Solartron 1286 DC potentiostat was used under controlled temperatures and in a humidity ramp down mode (from 98 to 20%), according to

previous finding.[32] Linear sweep voltammetry (BioLogic VSP, V= -0.1~ +0.1 V, sweep rate = 10 mV/s) was used to measure the membrane resistance in liquid water at ambient conditions.

Ionic conductivity, κ, of the membrane was calculated from:

$$\kappa = \frac{L}{R \times A} \quad (5)$$

where L is the distance of two Pt electrodes for measuring voltage, R is the membrane resistance, and A is the cross-sectional area of the membrane.

Ion conductivity can be expressed in terms of carrier concentration (e.g. imidazolium functional group) ($[\phi^-]$) and effective ion mobility (u_{X^-}) in the form of:

$$\kappa = F[\phi^-]u_{X^-} \quad (6)$$

where F denotes the Faraday constant.

Through-plane conductivity was measured by applying a DC sweep from 0 to 50 mV at a rate of 100 mV/s in KOH and K_2CO_3 electrolytes in a 4-probe configuration with two fixed Luggin capillaries placed ~1 mm from the membrane on each side with Ag/AgCl reference electrodes for the voltage sense and platinum mesh for the current carrying electrodes. The membrane conductivity was calculated by subtracting the membrane+solution resistance from the solution resistance.

2.7 Small Angle X-ray Scattering (SAXS)

Small-angle X-ray scattering (SAXS) experiments were performed in beamline 7.3.3 of the Advanced Light Source (ALS) at Lawrence Berkeley National Laboratory (LBNL). The X-ray wavelength used was $\lambda = 0.124$ nm, with a monochromator energy resolution of E/dE of 100, and the presented patterns were collected using a 2D Dectris Pilatus 2M CCD detector (172 μm × 172 μm pixel size). The scattering wave vector, $q = 4\pi \sin(\theta/2)/\lambda$, where θ is the scattering angle, was in the range of 0.001 to 0.04 $Å^{-1}$ for SAXS. SAXS images for dry and liquid-equilibrated samples were obtained *in-situ* using custom-designed temperature-controlled solution cells with X-ray transparent Kapton™ windows. Dry samples were sealed in sample holders after vacuum drying for 12 hr. For liquid-water experiments, samples were immersed in liquid water in the solution cells. All the experiments were carried out at 25 °C, and the samples were equilibrated overnight prior to imaging. The collected two-dimensional scattering patterns were azimuthally integrated to generate 1-D intensity profiles, I(q), which were corrected for background scattering.

3. Results and Discussions

3.1 Morphology

Morphology of ion-exchange membranes is a key characteristic that affects material properties. Nano/micro-phase separation, which is driven by the enthalpy associated with the de-mixing of incompatible components in polymers, can result in numerous distinct morphologies.[33] Ion-conducting polymers that exhibit phase-separated nanodomain networks are comprised of one phase that facilitates ion transport, while a second phase provides complementary functions like mechanical stability and integrity. However, many random ion-conducting copolymers, AEMs in particular, are weakly phase-separated or are completely amorphous, based on X-ray scattering techniques, including common AEMs such as Fumasep FAA-3[32, 34,35] and, as shown in this study, Sustainion.

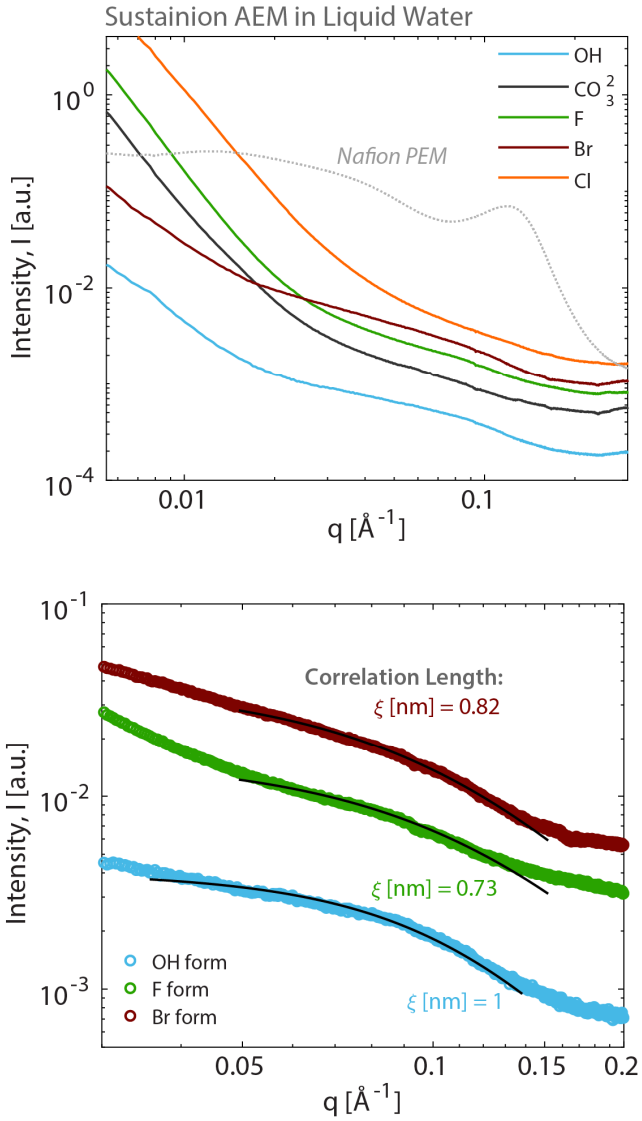

Figure 2 (a) SAXS spectra for Sustainion membranes with various counter-ion forms in liquid water at RT with Nafion included (gray dotted line). (b)Teubner-Strey fitting for OH^-, F^-, and Br^- forms.

Figure 2 shows the small-angle X-ray scattering (SAXS) profiles for Sustainion membranes in various counter-ions (anions). Even though Sustainion retains a predominantly amorphous structure for all anion forms, the impact of anions on the tendency to drive nano-phase separation can be obtained using the correlation length (ξ) estimated from the Tuebner-Strey two component scattering model (see SI for details).[36, 37] An increase in ξ observed with anion type, F^-< Br^-< OH^-, reflecting slight increased tendency for nano-phase separation, albeit not strongly, but is also

indicative of hydration where the ion form changes the degree of water uptake under ambient conditions. This lack of strong phase-separation can be attributed to the chemical architecture of these AEMs where chemical similarities between the different repeat units increase the likelihood of mixing (i.e. similar styrenic repeat units), even with the addition of the hydrophilic imidazole functional group. However, as discussed later, the correlation length is not only indicative of the hydration environment within the membrane but also the aqueous electrolyte environment with in the membrane.

3.2 Thermal and mechanical properties

The thermal degradation of membranes with and without an ePTFE reinforcement with a common counter ion (CO_3^{2-}) and in two important anion forms were examined using thermogravimetric analysis (TGA), as shown in Figure 3. Reinforcement was compared based on a consistent water content at beginning of test by drying the membrane at 120 °C briefly before a return to 30 °C where the mass loss collection begins with CO_3^{2-} chosen due ion stability in air. Compared to unreinforced Sustainion, the reinforced membrane exhibits a comparable mass loss (up to 200 °C) which is associated with tightly bound water in a similar vein to PEM-based membranes. Above 200 to 450 °C, there is a mass loss associated with the thermal decomposition of polymer's ionic groups and main (backbone) chains, which are consistent with previous reports of poly(styrene)s and poly(phenylene oxide)s based ionomers.[38] The reinforced membrane retains a slightly higher mass due to the presence of the ePTFE reinforcement until 450 °C where the Sustainion membrane undergoes a large mass loss. The thermal degradation of pristine ePTFE is also shown where the onset of degradation begins at 500 °C and ends at 600 °C. The overlapping mass percentage of the Sustainion membranes show agreement that all ePTFE is gone at this point in temperature and that the % mass difference between 450 and 500 °C is a reliable region to estimate mass fraction. The mass difference between 450 and 500 °C allows for an estimate ePTFE mass fraction of ~8.5%. This reinforcement fraction is comparable to the 8.9% obtained from the membrane density calculations and validated by SEM (SI-Table1 and Figure S4).

While CO_3^{2-} is stable in air, OH- form is the dominant ion used in electrochemical devices, and is of importance in this work, but reacts with CO_2 in air to convert to a mixture of CO_3^{2-}/HCO_3^-. Unlike the reinforcement comparison, data in Figure 3b are placed in the TGA crucible still

hydrated which leads to a large mass loss up to 100 °C with 35% and 58% mass loss for CO_3^{2-} and OH^- forms, respectively. The differences in water uptake are in agreement with the water uptake swelling isotherms, discussed below. Above 100 °C, there is a continuous mass loss with notable differences between the CO_3^{2-} and OH^- forms where the OH- form shows a double plateau, similar to the mass loss above 200 °C for CO_3^{2-} form in Figure 3a, but CO_3^{2-} form exhibits a single plateau. This distinction highlights that the state of the membrane at beginning of test is important where a CO_3^{2-} form membrane may have improved thermal degradation when water is present at start of test but exhibits a degradation mode at 200 °C when the test is started dry. Additionally, the OH- form membrane exhibits this degradation mode when 200 °C is reached, likely owing to the degradation susceptibility of the imidazolium functional group in the presence of hydroxides but also low water content.

High-temperature operation contributes to reduced overpotential of the proton exchange membrane-based water electrolyzer as a result of increased kinetics and membrane conductivity; however, operation is traditionally limited 20-80 °C due to the limitations of the proton conducting membrane (Nafion®).[9, 27] By operating near the glass transition temperature (T_g) of a polymer, especially under hydrated conditions where water plasticization can lower the T_g,[39] the increased chain mobility can affect other properties such as creep which can lead to constantly changing material properties due to thinning or even premature failure of devices. To examine the thermomechanical stability of AEMs in the dry state, their dynamical mechanical behavior is analyzed by DMA using a temperature sweep up to 300 °C (Figure 4). From DMA data, T_g of reinforced Sustainion and FAA3 membrane when dry is ~190 and 260 °C, respectively, which could enable a higher temperature operation than Nafion (with T_g ~ 110 °C) systems. The lower T_g of Sustainion compared to FAA3 is largely attributed to its respective unfunctionalized homopolymer (i.e. polystyrene vs. polyphenylene oxide).[40] Standard non-reinforced Sustainion membranes are excluded due to premature mechanical failure during mechanical testing (Figure S2).

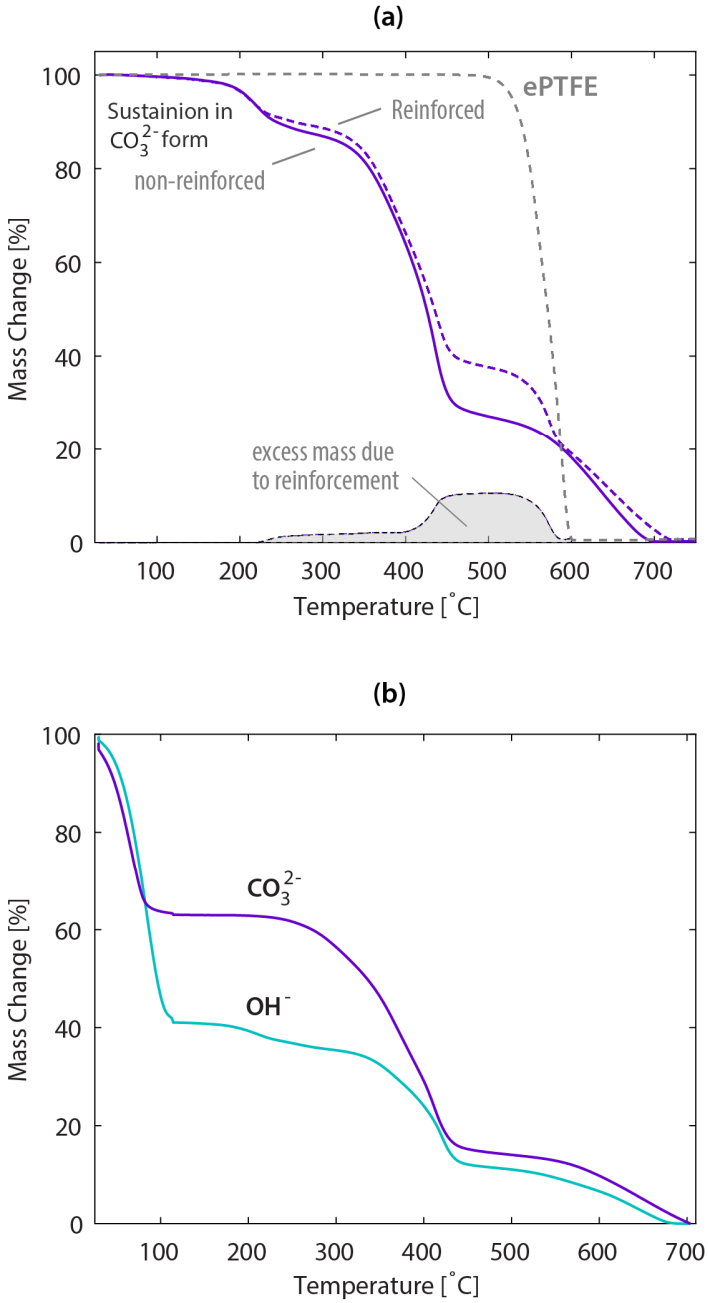

Figure 3 (a) TGA curves of unreinforced and reinforced Sustainion membranes in CO_3^{2-} form. The data for ePTFE material is also included for comparison. (b) Comparison of TGA profiles for unreinforced Sustainion in OH^- and CO_3^{2-} forms.

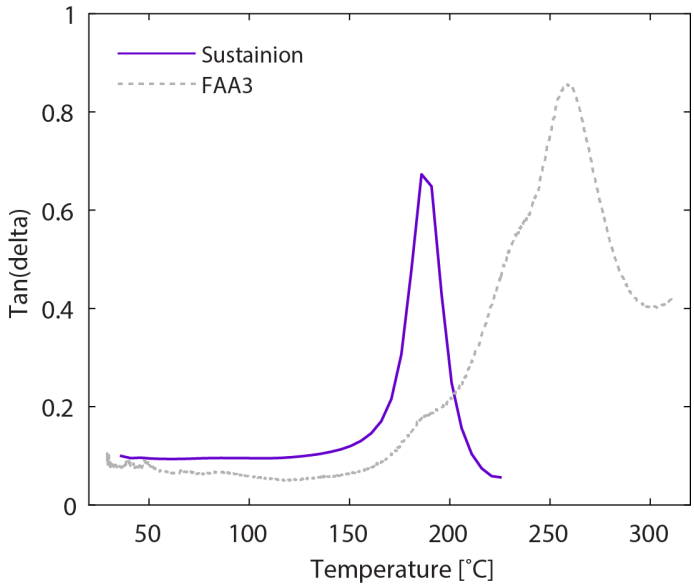

Figure 4 DMA profiles showing tan(delta) of reinforced Sustainion and Fumasep FAA3 membranes (CO_3^{2-}).

3.3 Water Uptake Behavior

Water uptake plays a significant role in membrane transport properties and cell performance, especially in AEM-based systems where water is used as a reactant and for improving cell performance by reducing Ohmic losses.[32, 41, 42] As shown in Figure 5, Sustainion obtains higher water content than FAA3 in both vapor and liquid saturated conditions. In vapor conditions, membranes in OH^- ion form exhibit higher water content than CO_3^{2-} form for both non-reinforced and reinforced membranes (Figure 5a). This can be attributed to the fact that (i) OH^- form has a greater number of water molecules in the first hydration shell per charge than CO_3^{2-}, ~5 vs ~4.5 for OH^- and CO_3^{2-}, respectively,[43] and (ii) the dissociation enthalpy of the corresponding salts where OH^- is easier to dissociate from the fixed charge group, resulting in increased water uptake at a given humidity.[44]

The impact of PTFE reinforcement on water sorption is also plotted in Figure 5. All reinforced membranes, regardless of their counter-anion, exhibited lower water content than non-reinforced membranes at all RH levels. The additional mechanical constraints imposed by the hydrophobic PTFE reinforcement and lower effective IEC arising from the presence of a hydrophobic support matrix lead to a 30% reduction in water content at high humidity.

In terms of saturated water capacity, all membranes show higher water content in liquid-equilibrated conditions compared to vapor-equilibrated conditions, regardless of reinforcement. This difference is commonly observed in proton exchange membranes and attributed to Schröder's paradox,[45] which has been a subject of debate, especially in PFSAs and fuel-cell applications with differing viewpoints based on thermodynamics and interfacial-structural phenomena. Interestingly, reinforced Sustainion shows a lower difference between liquid vs. vapor uptake (*i.e.,* less dependence on the equilibrium phase liquid vs. vapor) than the non-reinforced membrane, which could be due to reduced interfacial rearrangement as a result of confinement to the PTFE reinforcement and greater resistance to the lateral swelling.

Examination of sorption and desorption data indicates that both reinforced and non-reinforced Sustainion membranes exhibit lower sorption hysteresis than FAA3 (Figure S3). The water sorption hysteresis is associated with the stress relaxation of the cohesive force opposing swelling.[32, 46] The low sorption hysteresis was also found in crystalline materials and strong polyelectrolytes,[47] for which the sorption hysteresis was attributed to the polymer's resistance to plasticization by water (*i.e.,* stiffer chains) due to its higher shear modulus and the larger stress relaxation time consequently hampers the response to RH changes.[48] Compared to the non-reinforced membrane, reinforced Sustainion shows lower sorption hysteresis, which indicate reduced fluctuations in response to hydration difference that may arise during the cell operation. This finding could be beneficial for cold-start in vapor operation conditions, particularly for using the mitigation method of residual water removal from the system by gas purging,[49] where the residual free water is expected to be removed easier in the reinforced Sustainion.

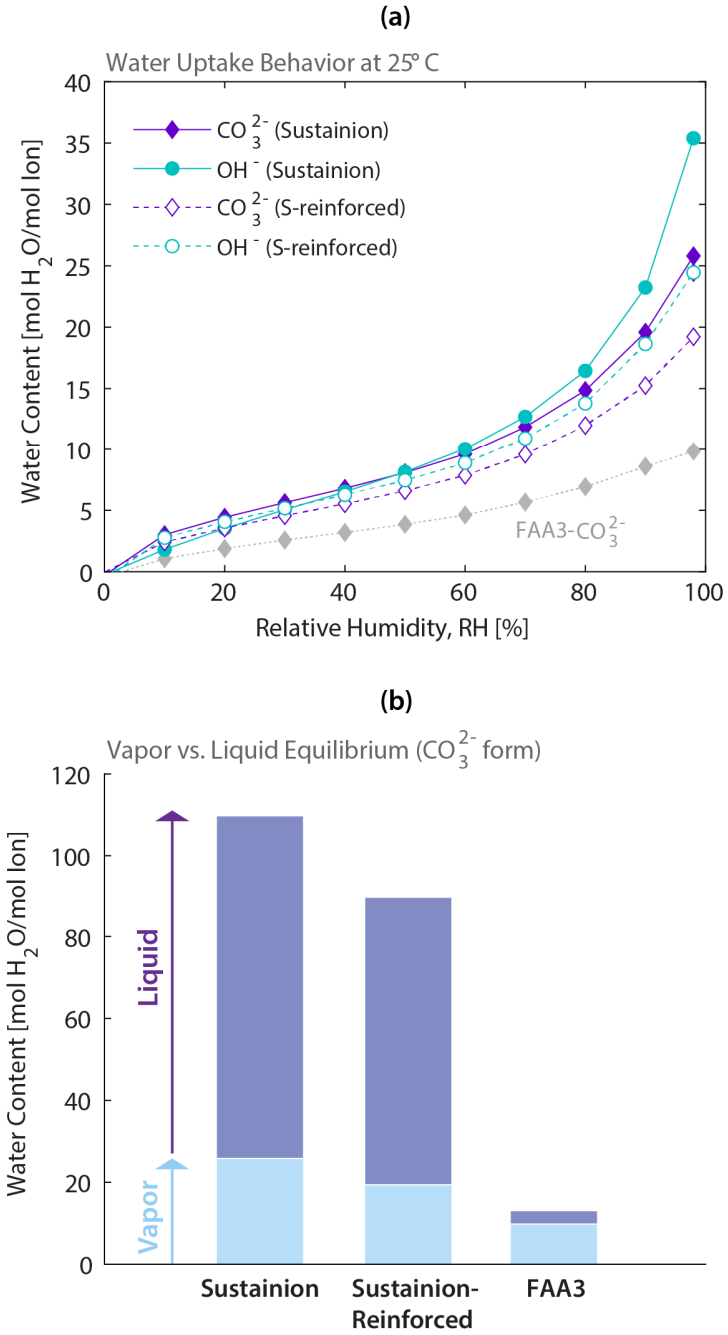

Figure 5. (a) Water vapor isotherm of Sustainion and FAA3 membranes in CO_3^{2-} and OH^- form at 25 °C, (b) Water uptake for vapor- and liquid-equilibrated membranes in CO_3^{2-} form.

3.4 Anion Conductivity

3.4.1 Effect of Hydration and Anions

Hydration plays a critical role in promoting ion conductivity and enhancing cell performance,[22, 41, 50] especially for AEMs that have amorphous structures[32, 51]. Anion conductivity (κ) of Sustainion increases monotonically with hydration and approaches the ion dilution at humidity values >90-95% RH, as shown in Figure 6. Compared to FAA3, Sustainion conductivity is >10x for OH^- and ~7x for CO_3^{2-} anions, which could explain the improved cell performance.[8, 18, 20] In fact, a recent AEM work found that ion conductivity plays the most critical role in the CO_2-related voltage loss from carbonation.[52]

Ion conductivity is governed by multiple factors, including ion concentration and mobility, tortuosity of transport pathways at the mesoscale, and electrostatic interactions and solvation energies at the nanoscale.[12, 32] Factors contributing to conductivity are determined as a function of water volume fraction, as shown in Figure 6(c-e). Compared to FAA3, Sustainion membranes show ~ 40% lower ion concentration range owing to their low IEC (Table 1), which translates into higher effective ion mobility for Sustainion – 10x higher than that for FAA3. This enhanced anion mobility explains the higher ion conductivity of Sustainion despite its lower ion concentration. One plausible explanation for the higher anion mobility of Sustainion is its more flexible polystyrene-based polymer chain with longer head group compared to the polyphenylene oxide (PPO) of FAA. This result highlights how the contributions from the ion concentration and effective ion mobility could modulate the effect of IEC when characterizing the ion transport in AEMs

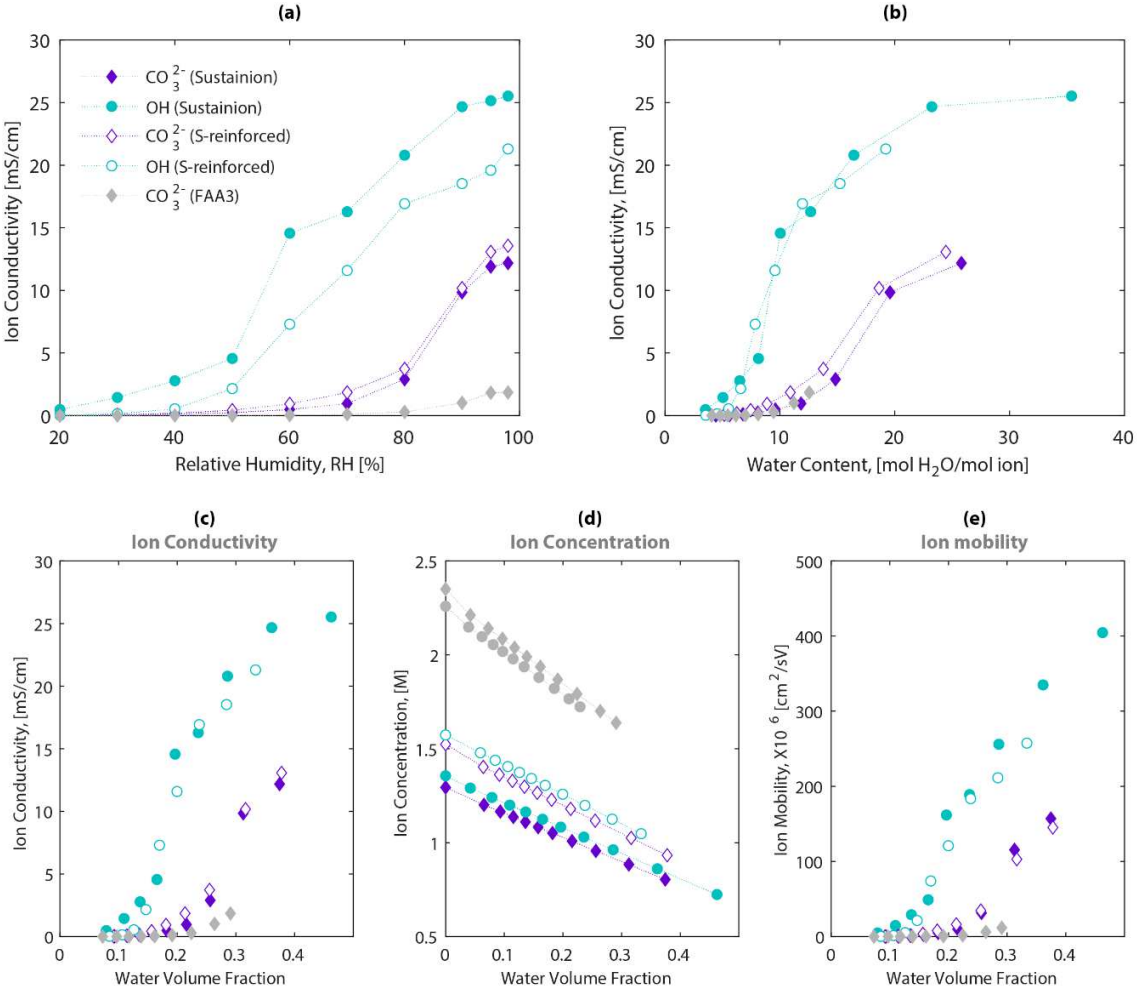

Figure 6 Ion conductivity as a function of (a) humidity, (b) water content, and (c) water volume fraction. The impact of water volume fraction on (d) analytical anion concentration (e) effective ion mobility for Sustainion membrane with various counter-ions. Baseline-FAA3 membranes are shown in gray.

To examine the impact of anion forms, Figure 7 shows the anion conductivity of the fully-hydrated AEMs normalized to the conductivity of anions in water at infinite dilution (κ/κ_o) plotted against AEM water content. AEMs with OH^- and CO_3^{2-} anions are the most relevant and common counter-ion forms in water and CO_2 electrolysis. Additionally, incorporating halide additives (e.g., I^-, Br^-, and Cl^-) into the liquid electrolyte (e.g., $CsHCO_3$) has been shown to improve the Cu catalyst selectivity for CO_2 electrolysis.[2, 53] However, the impact of Br- on the conductivity of the AEM separator was not addressed. Thus, AEMs exchanged with Br^- is also included in this comparison but is only included in liquid water measurements due to the nature of use (*i.e.* in aqueous

environments only). AEMs in Br^- form show significantly lower normalized conductivity compared to each AEM in OH^- and CO_3^{2-} form. The reduced conductivity imparted by the incorporation of halide additives into the system results in a trade-off between electrolysis performance of the membranes vs. enhanced catalyst efficiency. The normalized conductivity, κ/κ_o for all membranes of 3 anion forms (Br^-, OH^- and CO_3^{2-}) exhibits a universal increase with hydration, consistent with previous AEM studies.[32, 51] Thus, the fact that the normalized conductivity for different anions can be strongly related to hydration is of great practical and fundamental value for membrane design and implementation across the platforms.

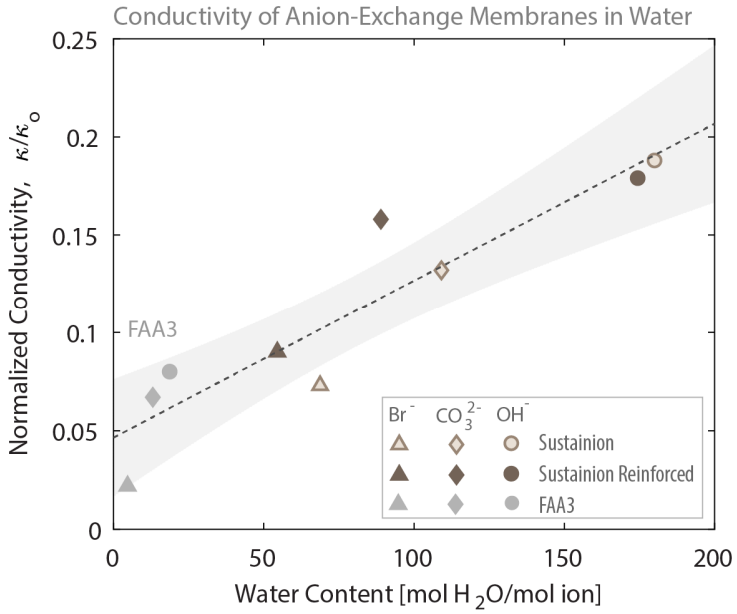

Figure 7 The ratio of conductivity to the conductivity at infinite dilution of ions (κ/κ_o) as a function of the water content of Sustainion at 25 °C in liquid water, FAA3 (shown in grey) is used as the baseline. The dashed line is a linear regression of all the data points shown with the 95% confidence interval (shaded region).

3.4.2 Effect of Temperature

As discussed in the previous section, Sustainion shows higher T_g than Nafion, which potentially allows for higher temperature operation. Figure 8 shows the impact of temperature on membrane anion conductivity. Conductivity increases monotonically with increasing temperature from 30 to 90 °C and peaks at 100 °C with high relative humidity (~90-100% RH). Additionally, the conductivity begins to converge to a maximum when humidity approaches 80% at 90 °C, suggesting that the previously discussed dilution effect begins to manifest at 80% RH.

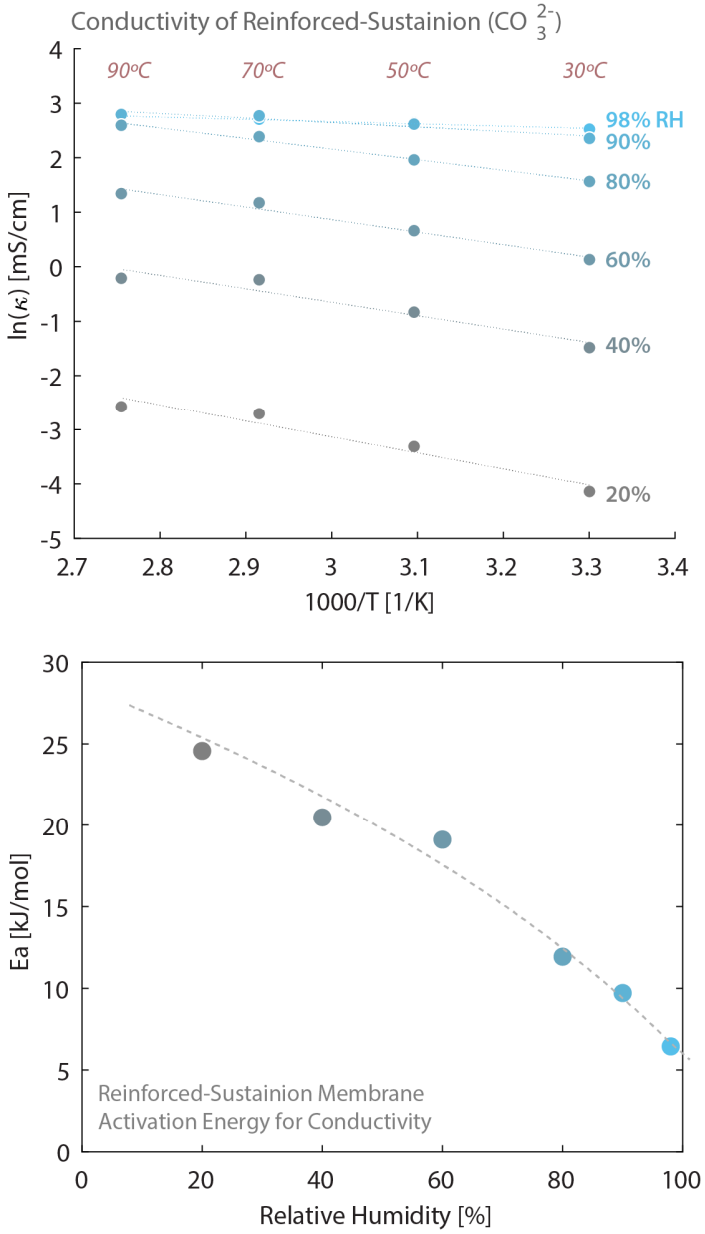

Figure 8 Ion conductivity of reinforced Sustainion membrane (CO_3^{2-}) plotted (a) as a function of relative humidity at different temperatures in Arrhenius form (b) activation energy (E_a) as a function of RH.

The carbonate ion transport activation energies (Ea) were obtained using (κ=A ($-Ea$/RT)), where A is a prefactor; R is the gas constant (8.314 J/mol/K), and T is the temperature (K). As shown in Figure 8b, at RH= 98%, Ea is calculated to be 6.4 kJ/mol, which is lower than literature values reported for poly(benzimidazolium) (PBI)[54] and poly(sulfones)[55] based ionomers. The

origin of the differences in Ea can be attributed to the faster ion transport of Sustainion as a result of the short backbone allowing two imidazolium groups from adjacent side chains to be in close proximity of each other, thereby making their first hydration shells overlap.[56] When increasing the humidity from 20% to 98% RH, Ea reduces by 74% as a result of increased hydration under high humidity conditions, indicating the degree of influence water has on anion transport in Sustainion. Nevertheless, from a membrane perspective, our study shows that operating at higher than 80 °C is possible for all humidity conditions but additional humidification at elevated temperatures may not improve performance due to ion dilution.

3.5 Impact of supporting electrolyte

Incorportation of supporting electrolytes into AEM systems have been found to improve device performance in several ways. For instance, when supporting electrolytes (SE) are incorporated into CO_2 reduction reaction and water electrolysis the catalyst performance can undergo significant improvements;[57] however, membrane properties are susceptible to the changing external environment (e.g. salt concentration and chemistry). Various water-soluble salts are employed as supporting electrolytes in CO_2R and water electrolysis including (bi)-carbonates, halides, and hydroxides.[58] Here, we report the impact of KOH and K_2CO_3 as supporting electrolytes on morphology and transport of Sustainion as these are the two most prominent anions in electrolysis.

Additional insights can be gain from membrane morphology as shown in Figure 9 where scattering was collected under different KOH concentrations for non-reinforced Sustainion. In the case of pure water, 0.5, and 1 M KOH solutions, a weak scattering peak is apparent at a q-value of 0.18 $Å^{-1}$ indicating a d-spacing of 3.4 nm for hydrophilic domains. When equilibrated in a 5 M an electrolyte , the membrane undergoes significant dehydration due to the lower water activity in the external electrolyte and a very strong scattering peak appears at 0.15 $Å^{-1}$ indicating increased d-spacing to 4.2 nm. While it is not clear why dehydration would lead to larger domains, it is possible that high electrolyte uptake, upwards of 300%, as discussed below, may disrupt or obscure pre-existing mixed-phase domains and could cause morphological changes at mesoscales. As water is removed from these membranes and replaced with KOH-rich electrolyte, the appearance of strong scattering from domains may appear due to the enhanced electron density difference (contrast) between the otherwise discernable phases. The formation of domains at high electrolyte

concentrations will add complexity to how conductivity values are interpreted. For instance, the presence of interconnected domains can induce a tortuosity factor, in turn, making ion transport through the membrane more difficult if not oriented in the preferred conduction direction.[45, 59] Alternatively, these hydrophilic domains may help conduction, as observed in the conductivity where K_2CO_3 plateaus while KOH continues to increase well into 4M concentrations. Well-defined domains in a membrane may contribute to further enhancing the membrane conductivity, overcoming the drawbacks of operating at high electrolytic concentrations.

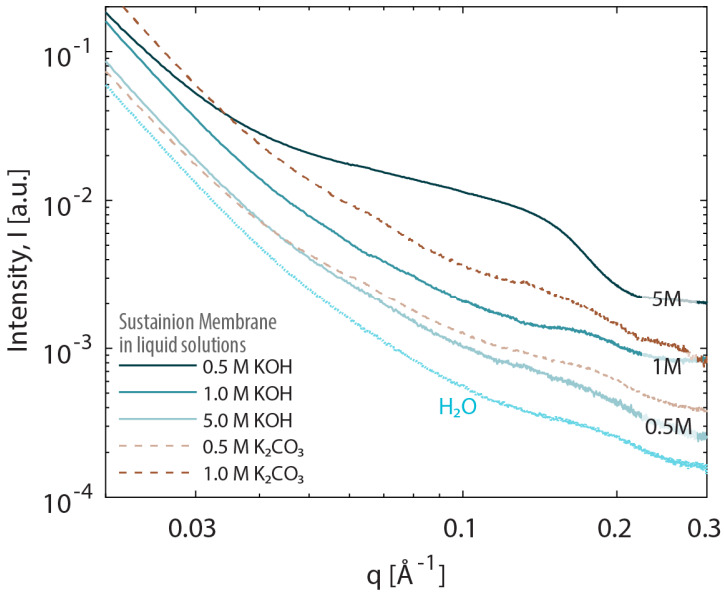

Figure 9 2D small-angle X-ray scattering of Sustainion membranes with various concentration of supporting electrolytes (KOH and K_2CO_3).

Figure 10a shows the effect of electrolyte concentration on the ion conductivity (κ) of unreinforced and reinforced Sustainion membranes where κ initially increases with increasing electrolyte concentration followed by a plateau. Increased conductivity agrees well with previously reported cell performance enhancement with increasing SE concentration due to reduced Ohmic resistance of the membrane.[60] External electrolyte concentrations above 0.1 M have been shown to overcome Donnan exclusion causing excess ions to exist within the membrane, providing a greater number of charge carriers for ion transport.[61] Values reported in this work under vapor equilibration at high humidity agree quite well with the conductivity values measured at 0.1 M KOH and K_2CO_3 especially when considering different sample geometries and environments.

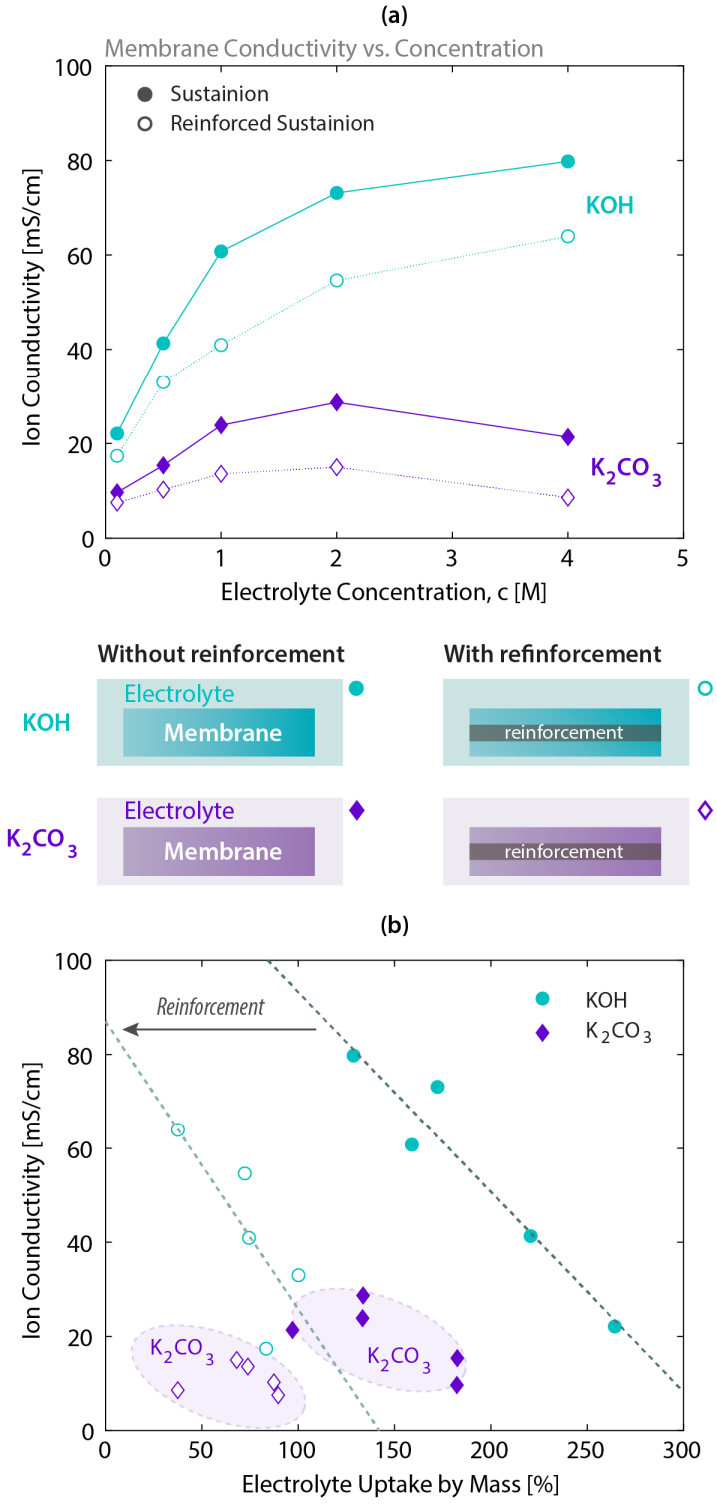

Figure 10 The impact of supporting electrolytes (KOH and K_2CO_3) concentration on Sustainion membranes (a) Anion conductivity as a function of supporting electrolyte concentration (b) anion conductivity plotted against the electrolyte mass uptake in the membrane. Dashed lines represent linear regression to each membrane in KOH.

When comparing the impact of electrolyte type (K_2CO_3 vs. KOH) and reinforcement, the conductivity undergoes differing degrees of changes depending on the framework. For K_2CO_3, κ increases over the electrolyte concentration range, with a peak conductivity of 27 and 13 mS/cm around 2 M for non-reinforced and reinforced membranes, respectively. When K_2CO_3 concentration is 4 M, a noticeable decrease in conductivity is observed, which may be related to (i) higher degrees of dehydration due to the lowered water activity of a 4 M solution, and/or (ii) increased viscosity of the electrolyte (Figure S5) and ion condensation[62] within the membrane slowing ion transport. KOH-equilibrated samples approached a plateau conductivity of 80 and 64 mS/cm at 4 M for non-reinforced and reinforced membranes, respectively, but does not achieve the same degree of viscosity increases of K_2CO_3 electrolytes.

Figure 10b shows the conductivity change with % mass uptake of the electrolyte in each membrane. Interestingly, significant decreases in electrolyte uptake (up to 2-3x) are observed with only modest losses in conductivity when reinforcement is incorporated into a Sustainion membrane. In particular, KOH electrolyte uptake is reduced by ~60%, while only a 25% reduction in conductivity is observed at electrolyte concentrations of 2 M. In the case of K_2CO_3, the electrolyte uptake and conductivity were both reduced by ~50%. Thus, presence of a reinforcement in an AEM could alter the way conductivity changes with the electrolyte uptake, albeit with a dependence also on the nature of the anions. Reinforcing the membrane provides a means of reducing lateral swelling and increasing mechanical stability but excess electrolyte still imbibes the membrane, resulting in enhanced transport properties. Lower electrolyte uptake at a given concentration would reduce crossover of unwanted species through the membrane without hampering the conductivity of the cell, thereby increasing the membrane selectivity.

The inter-related effects of external electrolyte and mechanical reinforcement could be a favorable outcome for electrolysis; however, the electrolyte concentrations where strong scattering is exhibited is generally outside the standard support electrolytes concentrations used (<1 M). Additionally, controlling selectivity of the membrane in certain application while enhancing the stability may be achieved thanks to the reinforcement layer. For instance, performance in AEM water electrolysis is markedly improved when incorporating support electrolytes over just pure deionized water with current densities greater than 2000 mA/cm^2 for a 1 M KOH solution but limited to a few hundred mA/cm^2 when using DI water.[63] However, a growing concern of water electrolysis is gas crossover which not only causes safety issues with H_2 concentration mixing in

an O_2 environment but also a reduced overall efficiency. Results shown here suggest that reinforcement can reduce polymer swelling while retaining high ion transport that impact energy efficiency but the reduced swelling may serve to mitigate gas crossover without sacrificing system efficiency that could be lost to gas crossover.

Conclusion

In this study, we investigated the impact of hydration, temperature, supporting electrolyte, ePTFE reinforcement, and counter-ion on the properties of Sustainion membranes. Compared to baseline FAA3, Sustainion shows much greater ion conductivity at all hydration conditions, possibly due to its better effective ion mobility. This high conductivity could be responsible for previously showed better cell performance using Sustainion. The ion conductivity of Sustainion is strongly dependent on hydration and operation temperature, and counter-anion. Our study shows the possibility of an operating cell at a temperature approaching 100 °C. The supporting electrolyte (SE) is found to have a substantial impact on membrane conductivity. Even though the amorphous structure doesn't change much with SE concentration until high SE concentrations are reached, the membrane conductivity increased significantly. ePTFE reinforcement is found to impact membrane mechanical, thermal and sorption, showing promise of enhancing cell performance but also reducing species crossover. Our findings provide not only important information that could explain reported cell performance improvements, but also offer critical design parameters for next-generation AEMs with enhanced electrolysis performance.

Acknowledgments

Funding for this work was provided by HydroGEN Consortium through the Hydrogen and Fuel Cell Technologies Office (HFTO), Office of Energy Efficiency and Renewable Energy, of the U.S. Department of Energy (DOE), under contract no. DE-AC02-05CH11231. We thank Nemanja Danilovic for insightful discussion. We also thank Chenhui Zhu and Eric Schaible for their assistance with facilitating the equipment at the Advanced Light Source (ALS) beamline 7.3.3, supported by the Office of Science, Office of Basic Energy Sciences, of the U.S. DOE (Contract No. DE-AC02-05CH11231).

CRediT Statement

X. Luo: Writing - Original Draft, Conceptualization, Investigation, Methodology.
D. Kushner: Writing - Review & Editing, Conceptualization, Investigation, Methodology, Formal analysis.
A. Kusoglu: Writing - Review & Editing, Data Curation, Visualization, Formal analysis, Supervision

References

(1) Bistline, J.; Abhyankar, N.; Blanford, G.; Clarke, L.; Fakhry, R.; McJeon, H.; Reilly, J.; Roney, C.; Wilson, T.; Yuan, M.; et al. Actions for reducing US emissions at least 50% by 2030. *Science* **2022**, *376* (6596), 922-924. DOI: 10.1126/science.abn0661.

(2) Gao, D.; Arán-Ais, R. M.; Jeon, H. S.; Roldan Cuenya, B. Rational catalyst and electrolyte design for CO2 electroreduction towards multicarbon products. *Nature Catalysis* **2019**, *2* (3), 198-210. DOI: 10.1038/s41929-019-0235-5.

(3) García de Arquer, F. P.; Dinh, C.-T.; Ozden, A.; Wicks, J.; McCallum, C.; Kirmani, A. R.; Nam, D.-H.; Gabardo, C.; Seifitokaldani, A.; Wang, X.; et al. CO₂ electrolysis to multicarbon products at activities greater than 1 A cm^{−2}. *Science* **2020**, *367* (6478), 661-666. DOI: 10.1126/science.aay4217.

(4) Kusoglu, A. (Re)Defining Clean Hydrogen: From Colors to Emissions. *The Electrochemical Society Interface* **2022**, *31* (4), 47. DOI: 10.1149/2.F08224IF.

(5) Bui, J. C.; Kim, C.; King, A. J.; Romiluyi, O.; Kusoglu, A.; Weber, A. Z.; Bell, A. T. Engineering Catalyst-Electrolyte Microenvironments to Optimize the Activity and Selectivity for the Electrochemical Reduction of CO(2) on Cu and Ag. *Acc Chem Res* **2022**, *55* (4), 484-494. DOI: 10.1021/acs.accounts.1c00650 From NLM Medline.

(6) Garg, S.; Giron Rodriguez, C. A.; Rufford, T. E.; Varcoe, J. R.; Seger, B. How membrane characteristics influence the performance of CO2 and CO electrolysis. *Energ Environ Sci* **2022**, 10.1039/D2EE01818G. DOI: 10.1039/d2ee01818g.

(7) Xu, W.; Scott, K.; Basu, S. Performance of a high temperature polymer electrolyte membrane water electrolyser. *Journal of Power Sources* **2011**, *196* (21), 8918-8924. DOI: https://doi.org/10.1016/j.jpowsour.2010.12.039.

(8) Kaczur, J. J.; Yang, H.; Liu, Z.; Sajjad, S. D.; Masel, R. I. Carbon Dioxide and Water Electrolysis Using New Alkaline Stable Anion Membranes. *Front Chem* **2018**, *6*, 263-263. DOI: 10.3389/fchem.2018.00263 PubMed.

(9) Shiva Kumar, S.; Himabindu, V. Hydrogen production by PEM water electrolysis – A review. *Materials Science for Energy Technologies* **2019**, *2* (3), 442-454. DOI: https://doi.org/10.1016/j.mset.2019.03.002.

(10) Alia, S.; Ding, D.; McDaniel, A.; Toma, F. M.; Dinh, H. N. Chalkboard 2 - How to Make Clean Hydrogen. *The Electrochemical Society Interface* **2021**, *30* (4), 49. DOI: 10.1149/2.F13214IF.

(11) Varcoe, J. R.; Atanassov, P.; Dekel, D. R.; Herring, A. M.; Hickner, M. A.; Kohl, P. A.; Kucernak, A. R.; Mustain, W. E.; Nijmeijer, K.; Scott, K.; et al. Anion-exchange membranes in electrochemical energy systems. *Energy & Environmental Science* **2014**, *7* (10), 3135-3191, 10.1039/C4EE01303D. DOI: 10.1039/C4EE01303D.

(12) Kim, Y. S. Polymer Electrolytes with High Ionic Concentration for Fuel Cells and Electrolyzers. *ACS Applied Polymer Materials* **2021**, *3* (3), 1250-1270. DOI: 10.1021/acsapm.0c01405.
(13) Carmo, M.; Fritz, D. L.; Mergel, J.; Stolten, D. A comprehensive review on PEM water electrolysis. *International Journal of Hydrogen Energy* **2013**, *38* (12), 4901-4934. DOI: 10.1016/j.ijhydene.2013.01.151.
(14) Kim, C.; Bui, J. C.; Luo, X.; Cooper, J. K.; Kusoglu, A.; Weber, A. Z.; Bell, A. T. Tailored catalyst microenvironments for CO2 electroreduction to multicarbon products on copper using bilayer ionomer coatings. *Nature Energy* **2021**, *6* (11), 1026-1034. DOI: 10.1038/s41560-021-00920-8.
(15) Marino, M. G.; Kreuer, K. D. Alkaline Stability of Quaternary Ammonium Cations for Alkaline Fuel Cell Membranes and Ionic Liquids. *ChemSusChem* **2015**, *8* (3), 513-523. DOI: 10.1002/cssc.201403022. Salvatore, D. A.; Gabardo, C. M.; Reyes, A.; O'Brien, C. P.; Holdcroft, S.; Pintauro, P.; Bahar, B.; Hickner, M.; Bae, C.; Sinton, D.; et al. Designing anion exchange membranes for CO2 electrolysers. *Nature Energy* **2021**, *6* (4), 339-348. DOI: 10.1038/s41560-020-00761-x. Moreno-González, M.; Mardle, P.; Zhu, S.; Gholamkhass, B.; Jones, S.; Chen, N.; Britton, B.; Holdcroft, S. One year operation of an anion exchange membrane water electrolyzer utilizing Aemion+® membrane: Minimal degradation, low H2 crossover and high efficiency. *Journal of Power Sources Advances* **2023**, *19*, 100109. DOI: 10.1016/j.powera.2023.100109.
(16) Chen, D.; Hickner, M. A.; Agar, E.; Kumbur, E. C. Optimizing membrane thickness for vanadium redox flow batteries. *Journal of Membrane Science* **2013**, *437*, 108-113. DOI: https://doi.org/10.1016/j.memsci.2013.02.007. Motealleh, B.; Liu, Z.; Masel, R. I.; Sculley, J. P.; Richard Ni, Z.; Meroueh, L. Next-generation anion exchange membrane water electrolyzers operating for commercially relevant lifetimes. *International Journal of Hydrogen Energy* **2021**, *46* (5), 3379-3386. DOI: https://doi.org/10.1016/j.ijhydene.2020.10.244.
(17) Douglin, J. C.; Varcoe, J. R.; Dekel, D. R. A high-temperature anion-exchange membrane fuel cell. *Journal of Power Sources Advances* **2020**, *5*, 100023. DOI: https://doi.org/10.1016/j.powera.2020.100023.
(18) Yang, H.; Kaczur, J. J.; Sajjad, S. D.; Masel, R. I. Electrochemical conversion of CO2 to formic acid utilizing Sustainion™ membranes. *Journal of CO2 Utilization* **2017**, *20*, 208-217. DOI: https://doi.org/10.1016/j.jcou.2017.04.011.
(19) Liu, Z.; Yang, H.; Kutz, R.; Masel, R. I. CO2 Electrolysis to CO and O2 at High Selectivity, Stability and Efficiency Using Sustainion Membranes. *Journal of The Electrochemical Society* **2018**, *165* (15), J3371-J3377. DOI: 10.1149/2.0501815jes.
(20) Liu, Z.; Sajjad, S.; Gao, Y.; Kaczur, J.; I.Masel, R. An Alkaline Water Electrolyzer with Sustainion™ Membranes: 1 A/cm² at 1.9V with Base Metal Catalysts. *ECS Transactions* **2017**, *77*, 71-73. DOI: 10.1149/07709.0071ecst.
(21) Li, F.; Thevenon, A.; Rosas-Hernández, A.; Wang, Z.; Li, Y.; Gabardo, C. M.; Ozden, A.; Dinh, C. T.; Li, J.; Wang, Y.; et al. Molecular tuning of CO2-to-ethylene conversion. *Nature* **2020**, *577* (7791), 509-513. DOI: 10.1038/s41586-019-1782-2. Pushkareva, I. V.; Pushkarev, A. S.; Grigoriev, S. A.; Modisha, P.; Bessarabov, D. G. Comparative study of anion exchange membranes for low-cost water electrolysis. *Int. J. Hydrogen Energy* **2020**, *45* (49), 26070-26079. DOI: 10.1016/j.ijhydene.2019.11.011. Lindquist, G. A.; Oener, S. Z.; Krivina, R.; Motz, A. R.; Keane, A.; Capuano, C.; Ayers, K. E.; Boettcher, S. W. Performance and Durability of Pure-

Water-Fed Anion Exchange Membrane Electrolyzers Using Baseline Materials and Operation. *ACS Appl Mater Interfaces* **2021**. DOI: 10.1021/acsami.1c06053.
(22) Wheeler, D. G.; Mowbray, B. A. W.; Reyes, A.; Habibzadeh, F.; He, J.; Berlinguette, C. P. Quantification of water transport in a CO2 electrolyzer. *Energy & Environmental Science* **2020**, 10.1039/D0EE02219E. DOI: 10.1039/D0EE02219E.
(23) Kutz, R. B.; Chen, Q.; Yang, H.; Sajjad, S. D.; Liu, Z.; Masel, I. R. Sustainion Imidazolium-Functionalized Polymers for Carbon Dioxide Electrolysis. *Energy Technology* **2017**, *5* (6), 929-936. DOI: doi:10.1002/ente.201600636. Henkensmeier, D.; Najibah, M.; Harms, C.; Žitka, J.; Hnát, J.; Bouzek, K. Overview: State-of-the Art Commercial Membranes for Anion Exchange Membrane Water Electrolysis. *Journal of Electrochemical Energy Conversion and Storage* **2020**, *18* (2). DOI: 10.1115/1.4047963 (acccessed 11/8/2020).
(24) Kerres, J. A. Development of ionomer membranes for fuel cells. *Journal of Membrane Science* **2001**, *185* (1), 3-27. DOI: https://doi.org/10.1016/S0376-7388(00)00631-1. Liu, F.; Yi, B.; Xing, D.; Yu, J.; Zhang, H. Nafion/PTFE composite membranes for fuel cell applications. *Journal of Membrane Science* **2003**, *212* (1), 213-223. DOI: https://doi.org/10.1016/S0376-7388(02)00503-3. Zhu, X.; Zhang, H.; Liang, Y.; Zhang, Y.; Luo, Q.; Bi, C.; Yi, B. Challenging reinforced composite polymer electrolyte membranes based on disulfonated poly(arylene ether sulfone)-impregnated expanded PTFE for fuel cell applications. *Journal of Materials Chemistry* **2007**, *17* (4), 386-397, 10.1039/B611690F. DOI: 10.1039/B611690F.
(25) Penner, R. M.; Martin, C. R. Ion Transporting Composite Membranes: I . Nafion-Impregnated Gore-Tex. *Journal of The Electrochemical Society* **1985**, *132* (2), 514-515. DOI: 10.1149/1.2113875. Kolde, J. A. Advanced Composite Polymer Electrolyte Fuel Cell Membranes. *ECS Proceedings Volumes* **1995**, *1995-23* (1), 193-201. DOI: 10.1149/199523.0193pv.
(26) Weng, L.-C.; Bell, A. T.; Weber, A. Z. Towards membrane-electrode assembly systems for CO2 reduction: a modeling study. *Energy & Environmental Science* **2019**, *12* (6), 1950-1968, 10.1039/C9EE00909D. DOI: 10.1039/C9EE00909D.
(27) Kai, J.; Saito, R.; Terabaru, K.; Li, H.; Nakajima, H.; Ito, K. Effect of Temperature on the Performance of Polymer Electrolyte Membrane Water Electrolysis: Numerical Analysis of Electrolysis Voltage Considering Gas/Liquid Two-Phase Flow. *Journal of The Electrochemical Society* **2019**, *166* (4), F246-F254. DOI: 10.1149/2.0521904jes.
(28) Pătru, A.; Binninger, T.; Pribyl, B.; Schmidt, T. J. Design Principles of Bipolar Electrochemical Co-Electrolysis Cells for Efficient Reduction of Carbon Dioxide from Gas Phase at Low Temperature. *Journal of The Electrochemical Society* **2019**, *166* (2), F34-F43. DOI: 10.1149/2.1221816jes.
(29) Milshtein, J. D.; Darling, R. M.; Drake, J.; Perry, M. L.; Brushett, F. R. The Critical Role of Supporting Electrolyte Selection on Flow Battery Cost. *J Electrochem Soc* **2017**, *164* (14), A3883-A3895. DOI: 10.1149/2.1031714jes. Kiessling, A.; Fornaciari, J. C.; Anderson, G.; Peng, X.; Gerstmayr, A.; Gerhardt, M.; McKinney, S.; Serov, A.; Weber, A. Z.; Kim, Y. S.; et al. Influence of Supporting Electrolyte on Hydroxide Exchange Membrane Water Electrolysis Performance: Catholyte. *J Electrochem Soc* **2022**, *169* (2). DOI: 10.1149/1945-7111/ac4fed. Hassan, N. U.; Zheng, Y.; Kohl, P. A.; Mustain, W. E. KOH vs Deionized Water Operation in Anion Exchange Membrane Electrolyzers. *J Electrochem Soc* **2022**, *169* (4). DOI: 10.1149/1945-7111/ac5f1d.
(30) Kraglund, M. R.; Carmo, M.; Schiller, G.; Ansar, S. A.; Aili, D.; Christensen, E.; Jensen, J. O. Ion-solvating membranes as a new approach towards high rate alkaline electrolyzers. *Energy*

694 *& Environmental Science* **2019**, *12* (11), 3313-3318, 10.1039/C9EE00832B. DOI:
695 10.1039/C9EE00832B.
696 (31) Vennekötter, J.-B.; Scheuermann, T.; Sengpiel, R.; Wessling, M. The electrolyte matters:
697 Stable systems for high rate electrochemical CO2 reduction. *Journal of CO2 Utilization* **2019**,
698 *32*, 202-213. DOI: https://doi.org/10.1016/j.jcou.2019.04.007. Aili, D.; Kraglund, M. R.;
699 Tavacoli, J.; Chatzichristodoulou, C.; Jensen, J. O. Polysulfone-polyvinylpyrrolidone blend
700 membranes as electrolytes in alkaline water electrolysis. *Journal of Membrane Science* **2020**,
701 *598*, 117674. DOI: https://doi.org/10.1016/j.memsci.2019.117674.
702 (32) Luo, X.; Rojas-Carbonell, S.; Yan, Y.; Kusoglu, A. Structure-transport relationships of
703 poly(aryl piperidinium) anion-exchange membranes: Eeffect of anions and hydration. *Journal of*
704 *Membrane Science* **2019**, 117680. DOI: https://doi.org/10.1016/j.memsci.2019.117680.
705 (33) Bates, F. S.; Fredrickson, G. H. Block Copolymer Thermodynamics: Theory and
706 Experiment. *Annual Review of Physical Chemistry* **1990**, *41* (1), 525-557. DOI:
707 10.1146/annurev.pc.41.100190.002521. Bates, F. S.; Fredrickson, G. H. Block copolymers--
708 designer soft materials. *Physics Today* **1999**, *52*, 32.
709 (34) Schibli, E. M.; Wright, A. G.; Holdcroft, S.; Frisken, B. J. Morphology of Anion-
710 Conducting Ionenes Investigated by X-ray Scattering and Simulation. *The Journal of Physical*
711 *Chemistry B* **2018**, *122* (5), 1730-1737. DOI: 10.1021/acs.jpcb.7b10177. Kushner, D. I.; Zhu, L.;
712 Kusoglu, A.; Hickner, M. A. Side Chain Influence on the Mechanical Properties and Water
713 Uptake of Confined Comb-Shaped Cationic Polymer Thin Films. *Macromolecular Chemistry*
714 *and Physics* **2016**, *217* (21), 2442-2451. DOI: 10.1002/macp.201600254.
715 (35) Robertson, N. J.; Kostalik, H. A.; Clark, T. J.; Mutolo, P. F.; Abruña, H. D.; Coates, G. W.
716 Tunable High Performance Cross-Linked Alkaline Anion Exchange Membranes for Fuel Cell
717 Applications. *Journal of the American Chemical Society* **2010**, *132* (10), 3400-3404. DOI:
718 10.1021/ja908638d.
719 (36) Rojas, A. A.; Thakker, K.; McEntush, K. D.; Inceoglu, S.; Stone, G. M.; Balsara, N. P.
720 Dependence of Morphology, Shear Modulus, and Conductivity on the Composition of Lithiated
721 and Magnesiated Single-Ion-Conducting Block Copolymer Electrolytes. *Macromolecules* **2017**,
722 *50* (21), 8765-8776. DOI: 10.1021/acs.macromol.7b01686.
723 (37) Teubner, M.; Strey, R. Origin of the scattering peak in microemulsions. *The Journal of*
724 *Chemical Physics* **1987**, *87* (5), 3195-3200. DOI: 10.1063/1.453006.
725 (38) Mohanty, A. D.; Ryu, C. Y.; Kim, Y. S.; Bae, C. Stable Elastomeric Anion Exchange
726 Membranes Based on Quaternary Ammonium-Tethered Polystyrene-b-poly(ethylene-co-
727 butylene)-b-polystyrene Triblock Copolymers. *Macromolecules* **2015**, *48* (19), 7085-7095. DOI:
728 10.1021/acs.macromol.5b01382. Li, N.; Leng, Y.; Hickner, M. A.; Wang, C.-Y. Highly Stable,
729 Anion Conductive, Comb-Shaped Copolymers for Alkaline Fuel Cells. *Journal of the American*
730 *Chemical Society* **2013**, *135* (27), 10124-10133. DOI: 10.1021/ja403671u.
731 (39) Kim, Y. S.; Dong, L.; Hickner, M. A.; Glass, T. E.; Webb, V.; McGrath, J. E. State of Water
732 in Disulfonated Poly(arylene ether sulfone) Copolymers and a Perfluorosulfonic Acid
733 Copolymer (Nafion) and Its Effect on Physical and Electrochemical Properties. *Macromolecules*
734 **2003**, *36* (17), 6281-6285. DOI: 10.1021/ma0301451.
735 (40) Eisenberg, A.; Hird, B.; Moore, R. B. A New Multiplet-Cluster Model for the Morphology
736 of Random Ionomers. *Macromolecules* **1990**, *23* (18), 4098-4107.
737 (41) Diesendruck, C. E.; Dekel, D. R. Water – A key parameter in the stability of anion exchange
738 membrane fuel cells. *Current Opinion in Electrochemistry* **2018**, *9*, 173-178. DOI:
739 10.1016/j.coelec.2018.03.019. Dekel, D. R.; Amar, M.; Willdorf, S.; Kosa, M.; Dhara, S.;

740 Diesendruck, C. E. Effect of Water on the Stability of Quaternary Ammonium Groups for Anion
741 Exchange Membrane Fuel Cell Applications. *Chemistry of Materials* **2017**, *29* (10), 4425-4431.
742 DOI: 10.1021/acs.chemmater.7b00958. Omasta, T. J.; Mustain, W. E. Water and Ion Transport
743 in Anion Exchange Membrane Fuel Cells. In *Anion Exchange Membrane Fuel Cells: Principles,*
744 *Materials and Systems*, An, L., Zhao, T. S. Eds.; Springer International Publishing, 2018; pp 1-
745 31.
746 (42) Mandal, M.; Huang, G.; Hassan, N. U.; Peng, X.; Gu, T.; Brooks-Starks, A. H.; Bahar, B.;
747 Mustain, W. E.; Kohl, P. A. The Importance of Water Transport in High Conductivity and High-
748 Power Alkaline Fuel Cells. *Journal of The Electrochemical Society* **2019**, *167* (5), 054501. DOI:
749 10.1149/2.0022005jes.
750 (43) Botti, A.; Bruni, F.; Imberti, S.; Ricci, M. A.; Soper, A. K. Solvation of hydroxyl ions in
751 water. *The Journal of Chemical Physics* **2003**, *119* (10), 5001-5004. DOI: 10.1063/1.1605947.
752 (44) Marino, M. G.; Melchior, J. P.; Wohlfarth, A.; Kreuer, K. D. Hydroxide, halide and water
753 transport in a model anion exchange membrane. *J. Membr. Sci.* **2014**, *464*, 61-71. DOI:
754 10.1016/j.memsci.2014.04.003.
755 (45) Kusoglu, A.; Weber, A. Z. New Insights into Perfluorinated Sulfonic-Acid Ionomers. *Chem*
756 *Rev* **2017**, *117* (3), 987-1104. DOI: 10.1021/acs.chemrev.6b00159.
757 (46) Watt, I. C. Adsorption-Desorption Hysteresis in Polymers. *Journal of Macromolecular*
758 *Science: Part A - Chemistry* **1980**, *14* (2), 245-255. DOI: 10.1080/00222338008066635.
759 Jeromenok, J.; Weber, J. Restricted Access: On the Nature of Adsorption/Desorption Hysteresis
760 in Amorphous, Microporous Polymeric Materials. *Langmuir : the ACS journal of surfaces and*
761 *colloids* **2013**, *29* (42), 12982-12989. DOI: 10.1021/la402630s.
762 (47) Palmer, J. C.; Debenedetti, P. G. Computer Simulation of Water Sorption on Flexible
763 Protein Crystals. *The Journal of Physical Chemistry Letters* **2012**, *3* (18), 2713-2718. DOI:
764 10.1021/jz301118g. Kim, S. B.; Singh, R. S.; Paul, P. K. C.; Debenedetti, P. G. Effects of
765 disulfide bridges and backbone connectivity on water sorption by protein matrices. *Scientific*
766 *Reports* **2017**, *7* (1), 7957. DOI: 10.1038/s41598-017-08561-2. Bryan, W. P. Thermodynamic
767 models for water–protein sorption hysteresis. *Biopolymers* **1987**, *26* (10), 1705-1716. DOI:
768 doi:10.1002/bip.360261005.
769 (48) Lee, S.-W.; Lee, D. Integrated Study of Water Sorption/Desorption Behavior of Weak
770 Polyelectrolyte Layer-by-Layer Films. *Macromolecules* **2013**, *46* (7), 2793-2799. DOI:
771 10.1021/ma400076d.
772 (49) Zhang, J.; Zhang, H.; Wu, J.; Zhang, J. Chapter 11 - Fuel Cell Degradation and Failure
773 Analysis. In *Pem Fuel Cell Testing and Diagnosis*, Zhang, J., Zhang, H., Wu, J., Zhang, J. Eds.;
774 Elsevier, 2013; pp 283-335.
775 (50) Huang, G.; Mandal, M.; Peng, X.; Yang-Neyerlin, A. C.; Pivovar, B. S.; Mustain, W. E.;
776 Kohl, P. A. Composite Poly(norbornene) Anion Conducting Membranes for Achieving
777 Durability, Water Management and High Power (3.4 W/cm2) in Hydrogen/Oxygen Alkaline
778 Fuel Cells. *J. Electrochem. Soc.* **2019**, *166* (10), F637-F644. DOI: 10.1149/2.1301910jes.
779 Eriksson, B.; Grimler, H.; Carlson, A.; Ekström, H.; Wreland Lindström, R.; Lindbergh, G.;
780 Lagergren, C. Quantifying water transport in anion exchange membrane fuel cells. *International*
781 *Journal of Hydrogen Energy* **2019**, *44* (10), 4930-4939. DOI:
782 https://doi.org/10.1016/j.ijhydene.2018.12.185. Zheng, Y.; Ash, U.; Pandey, R. P.; Ozioko, A.
783 G.; Ponce-González, J.; Handl, M.; Weissbach, T.; Varcoe, J. R.; Holdcroft, S.; Liberatore, M.
784 W.; et al. Water Uptake Study of Anion Exchange Membranes. *Macromolecules* **2018**. DOI:
785 10.1021/acs.macromol.8b00034.

(51) Lu, J.; Barnett, A.; Molinero, V. Effect of Polymer Architecture on the Nanophase Segregation, Ionic Conductivity, and Electro-Osmotic Drag of Anion Exchange Membranes. *The Journal of Physical Chemistry C* **2019**, *123* (14), 8717-8726. DOI: 10.1021/acs.jpcc.9b01165. Giffin, G. A.; Lavina, S.; Pace, G.; Di Noto, V. Interplay between the Structure and Relaxations in Selemion AMV Hydroxide Conducting Membranes for AEMFC Applications. *The Journal of Physical Chemistry C* **2012**, *116* (45), 23965-23973. DOI: 10.1021/jp3094879.
(52) Zheng, Y.; Irizarry Colon, L. N.; Ul Hassan, N.; Williams, E. R.; Stefik, M.; LaManna, J. M.; Hussey, D. S.; Mustain, W. E. Effect of Membrane Properties on the Carbonation of Anion Exchange Membrane Fuel Cells. *Membranes (Basel)* **2021**, *11* (2). DOI: 10.3390/membranes11020102.
(53) Gao, D.; Scholten, F.; Roldan Cuenya, B. Improved CO2 Electroreduction Performance on Plasma-Activated Cu Catalysts via Electrolyte Design: Halide Effect. *ACS Catalysis* **2017**, *7* (8), 5112-5120. DOI: 10.1021/acscatal.7b01416.
(54) Wright, A. G.; Fan, J.; Britton, B.; Weissbach, T.; Lee, H.-F.; Kitching, E. A.; Peckham, T. J.; Holdcroft, S. Hexamethyl-p-terphenyl poly(benzimidazolium): a universal hydroxide-conducting polymer for energy conversion devices. *Energy & Environmental Science* **2016**, *9* (6), 2130-2142, 10.1039/C6EE00656F. DOI: 10.1039/C6EE00656F.
(55) Yan, J.; Hickner, M. A. Anion Exchange Membranes by Bromination of Benzylmethyl-Containing Poly(sulfone)s. *Macromolecules* **2010**, *43* (5), 2349-2356. DOI: 10.1021/ma902430y.
(56) Chen, C.; Tse, Y.-L. S.; Lindberg, G. E.; Knight, C.; Voth, G. A. Hydroxide Solvation and Transport in Anion Exchange Membranes. *Journal of the American Chemical Society* **2016**, *138* (3), 991-1000. DOI: 10.1021/jacs.5b11951.
(57) König, M.; Vaes, J.; Klemm, E.; Pant, D. Solvents and Supporting Electrolytes in the Electrocatalytic Reduction of CO2. *iScience* **2019**, *19*, 135-160. DOI: https://doi.org/10.1016/j.isci.2019.07.014.
(58) Singh, M. R.; Kwon, Y.; Lum, Y.; Ager, J. W.; Bell, A. T. Hydrolysis of Electrolyte Cations Enhances the Electrochemical Reduction of CO2 over Ag and Cu. *Journal of the American Chemical Society* **2016**, *138* (39), 13006-13012. DOI: 10.1021/jacs.6b07612. Varela, A. S.; Kroschel, M.; Reier, T.; Strasser, P. Controlling the selectivity of CO2 electroreduction on copper: The effect of the electrolyte concentration and the importance of the local pH. *Catalysis Today* **2016**, *260*, 8-13, Article. DOI: 10.1016/j.cattod.2015.06.009 Scopus. Dinh, C.-T.; Burdyny, T.; Kibria, M. G.; Seifitokaldani, A.; Gabardo, C. M.; García de Arquer, F. P.; Kiani, A.; Edwards, J. P.; De Luna, P.; Bushuyev, O. S.; et al. CO₂ electroreduction to ethylene via hydroxide-mediated copper catalysis at an abrupt interface. *Science* **2018**, *360* (6390), 783-787. DOI: 10.1126/science.aas9100.
(59) Crothers, A. R.; Darling, R. M.; Kusoglu, A.; Radke, C. J.; Weber, A. Z. Theory of Multicomponent Phenomena in Cation-Exchange Membranes: Part II. Transport Model and Validation. *J. Electrochem. Soc.* **2020**, *167* (1), 013548. DOI: 10.1149/1945-7111/ab6724. Kushner, D. I.; Crothers, A. R.; Kusoglu, A.; Weber, A. Z. Transport phenomena in flow battery ion-conducting membranes. *Current Opinion in Electrochemistry* **2020**, *21*, 132-139. DOI: 10.1016/j.coelec.2020.01.010.
(60) Gurudayal; Bullock, J.; Srankó, D. F.; Towle, C. M.; Lum, Y.; Hettick, M.; Scott, M. C.; Javey, A.; Ager, J. Efficient solar-driven electrochemical CO2 reduction to hydrocarbons and oxygenates. *Energy & Environmental Science* **2017**, *10* (10), 2222-2230, 10.1039/C7EE01764B. DOI: 10.1039/C7EE01764B.

(61) Beers, K. M.; Hallinan, D. T.; Wang, X.; Pople, J. A.; Balsara, N. P. Counterion Condensation in Nafion. *Macromolecules* **2011**, *44* (22), 8866-8870. DOI: 10.1021/ma2015084 (acccessed 2012/10/08).
(62) Bordi, F.; Colby, R. H.; Cametti, C.; De Lorenzo, L.; Gili, T. Electrical Conductivity of Polyelectrolyte Solutions in the Semidilute and Concentrated Regime: The Role of Counterion Condensation. *J Phys Chem B* **2002**, *106* (27), 6887-6893. DOI: 10.1021/jp020262i.
(63) Kiessling, A.; Fornaciari, J. C.; Anderson, G.; Peng, X.; Gerstmayr, A.; Gerhardt, M. R.; McKinney, S.; Serov, A.; Kim, Y. S.; Zulevi, B.; et al. Influence of Supporting Electrolyte on Hydroxide Exchange Membrane Water Electrolysis Performance: Anolyte. *J Electrochem Soc* **2021**, *168* (8). DOI: 10.1149/1945-7111/ac1dcd.
(64) Dudenas, P. J.; Kusoglu, A. Evolution of Ionomer Morphology from Dispersion to Film: An in Situ X-ray Study. *Macromolecules* **2019**, *52* (20), 7779-7785. DOI: 10.1021/acs.macromol.9b01024.